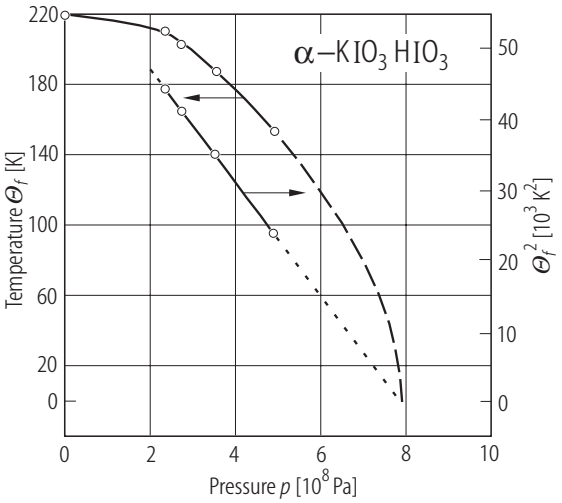

Fig. 32A-3-001. α-$KIO_3 \cdot HIO_3$. Θ_f, Θ_f^2 vs. p [87Bai].

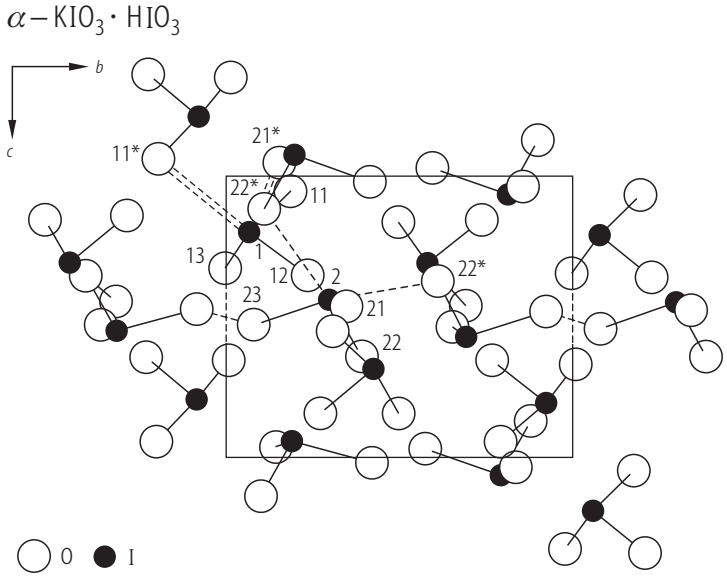

Fig. 32A-3-002. α-$KIO_3 \cdot HIO_3$. Crystal structure of phase I at RT [78Tre2]. Projection along the *a* axis. Only the iodate groups are shown. Used crystallographic axes are (*a*′, *b*′, *c*′), the second setting of cell defined in 3b.

$\alpha - KIO_3 \cdot HIO_3$

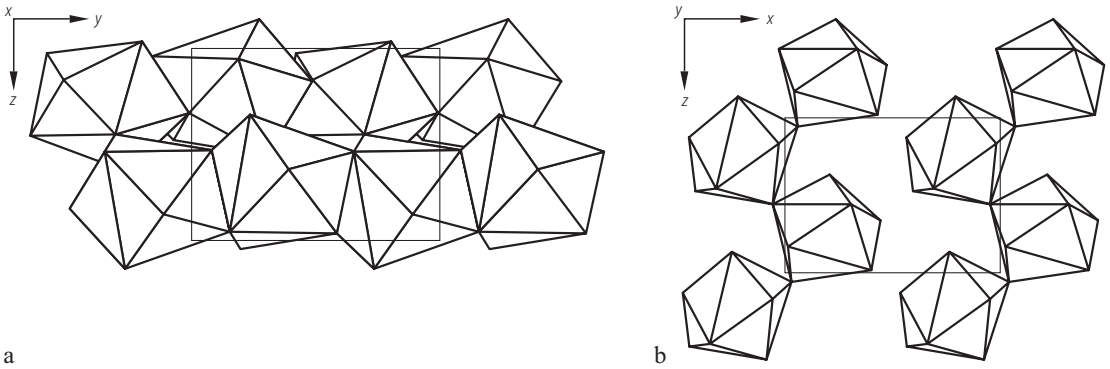

a b

Fig. 32A-3-003. α-$KIO_3 \cdot HIO_3$. Crystal structure of phase I at RT [78Tre2]. KO_9 polyhedra. (**a**) Projection along the *a* axis, (**b**) projection of polyhedra at a level $y \approx 0.25$ along the *b* axis. Used crystallographic axes are (*a′*, *b′*, *c′*), the second setting of cell defined in 3b.

$\alpha - KIO_3 \cdot HIO_3$

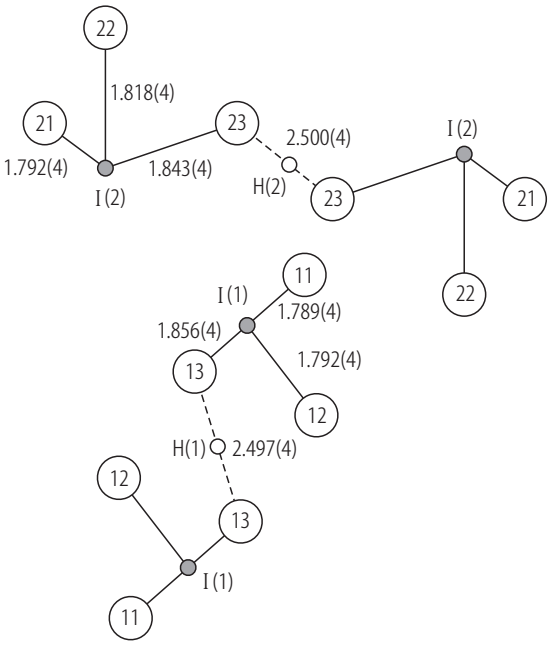

Fig. 32A-3-004. α-$KIO_3 \cdot HIO_3$. Crystal structure of phase I at RT [79Tre]. Structure of non-equivalent dimers of iodate. Distances in [Å].

$\beta - KIO_3 \cdot HIO_3$

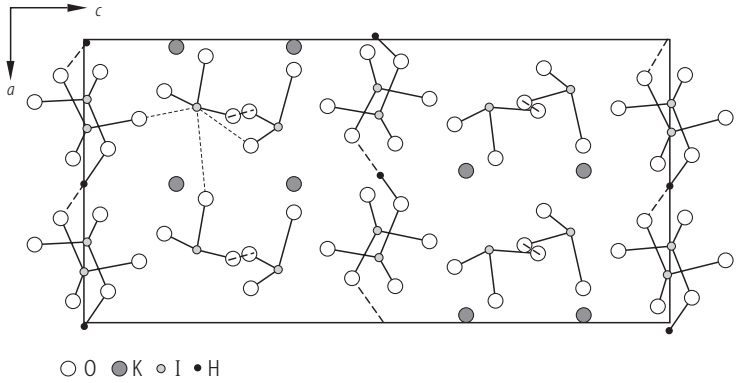

Fig. 32A-3-005. β-$KIO_3 \cdot HIO_3$. Crystal structure at RT [85Sor]. Projection along the *b* axis. Dashed lines: I–O bonds from second coordination sphere; dotted lines: hydrogen bonds.

$\gamma - KIO_3 \cdot HIO_3$

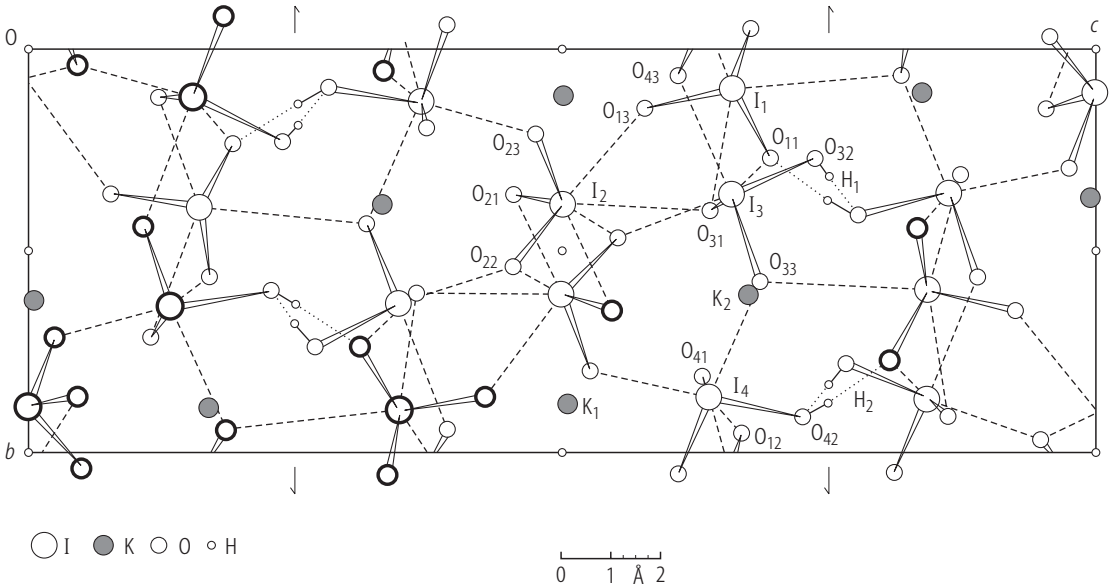

Fig. 32A-3-006. γ-$KIO_3 \cdot HIO_3$. Crystal structure at RT [72Kem]. Projection along the *a* axis. Dotted lines indicate hydrogen bonds; dashed lines weak I...O interactions.

$\delta - KIO_3 \cdot HIO_3$

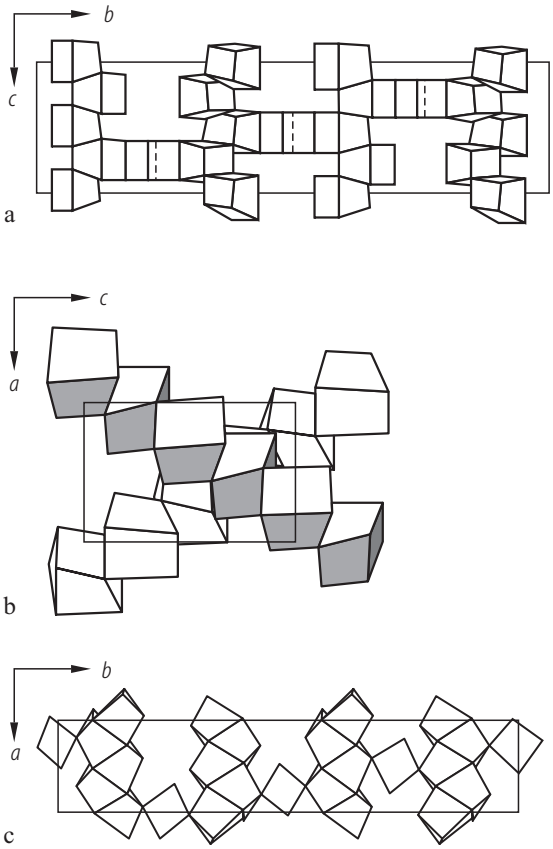

Fig. 32A-3-007. δ-KIO_3 · HIO_3. Crystal structure at RT [78Ily]. Fragments of three-dimensional framework of KO_8 polyhedra. (**a**) Chain of K(1) polyhedra and K(2) link; (**b**) cross section of framework parallel to (010); (**c**) projection along the *c* axis.

$\delta - KIO_3 \cdot HIO_3$

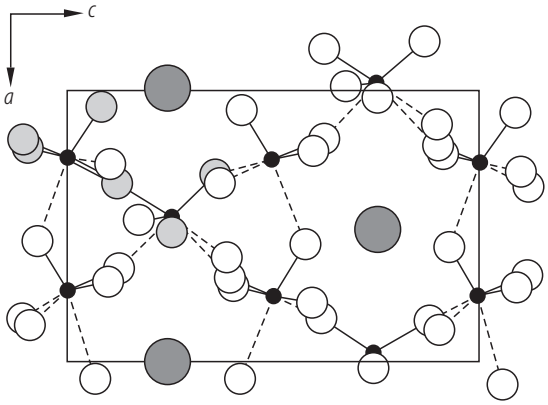

Fig. 32A-3-008. δ-KIO_3 · HIO_3. Crystal structure at RT [78Ily]. Projection along the *b* axis. A layer of structure $z \approx 0...0.125$ is shown. The large circles are K atoms. The dashed lines are "external" contacts. The dimer atoms are shaded, the contact I(1)–O(32)–I(3) is denoted by the double line.

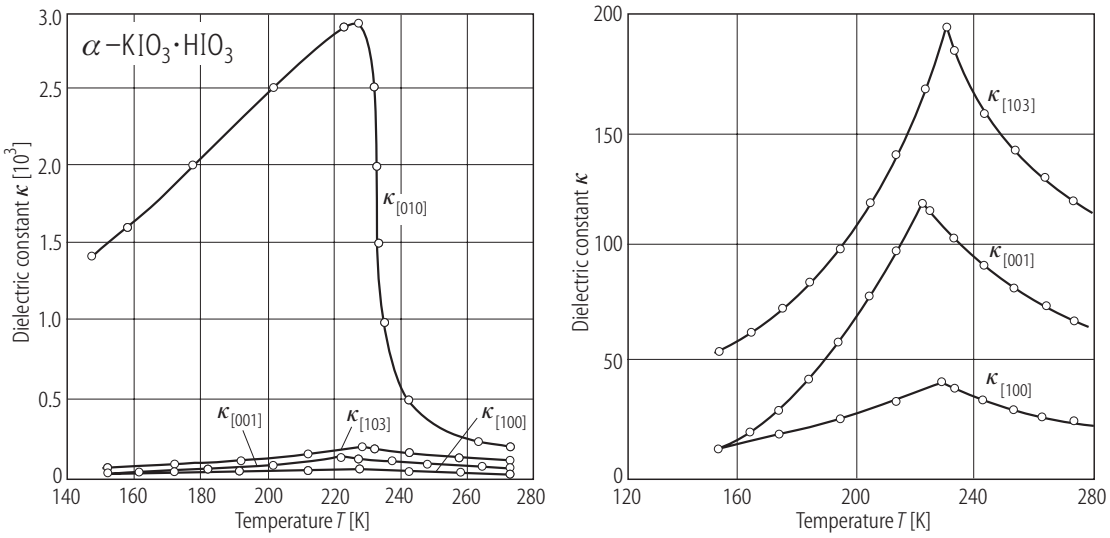

Fig. 32A-3-009. α-KIO_3 · HIO_3. κ vs. T along [010], [100], [001], [103] [78Pet1]. f = 1 kHz. Right panel shows details of $\kappa_{[103]}$, $\kappa_{[001]}$, $\kappa_{[100]}$ near Θ_f.

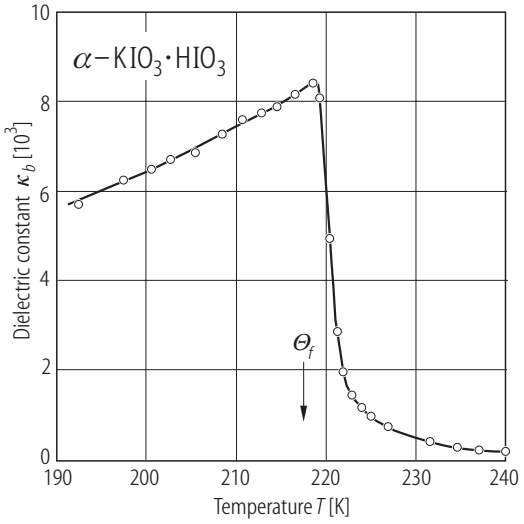

Fig. 32A-3-010. α-KIO_3 · HIO_3. κ_b vs. T [87Bai]. f = 230 kHz.

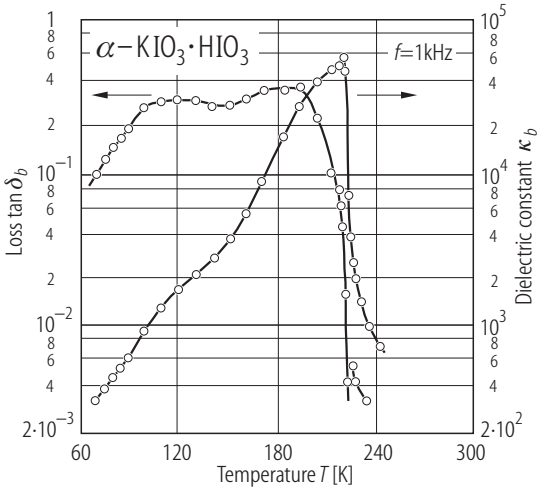

Fig. 32A-3-011. α-$KIO_3 \cdot HIO_3$. κ_b, $\tan\delta_b$ vs. T [87Bai]. f = 1 kHz.

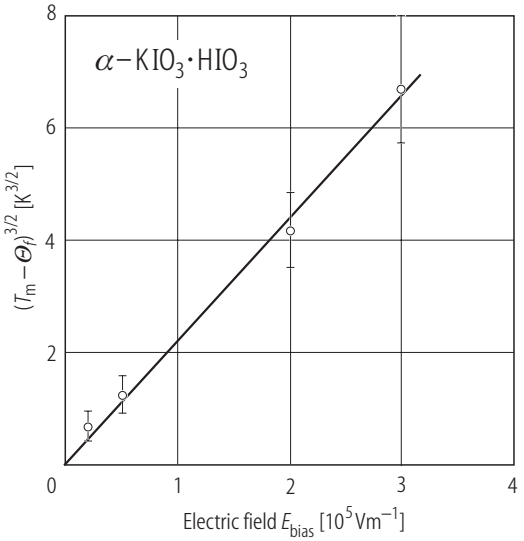

Fig. 32A-3-012. α-$KIO_3 \cdot HIO_3$. $(T_m - \Theta_f)^{3/2}$ vs. E_{bias} [91Bai]. T_m: temperature of maximum κ_b.

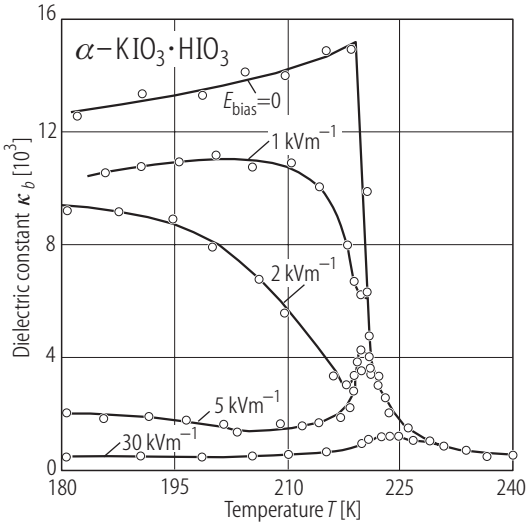

Fig. 32A-3-013. α-$KIO_3 \cdot HIO_3$. κ_b vs. T [91Bai]. Parameter: E_{bias}. f = 1 kHz.

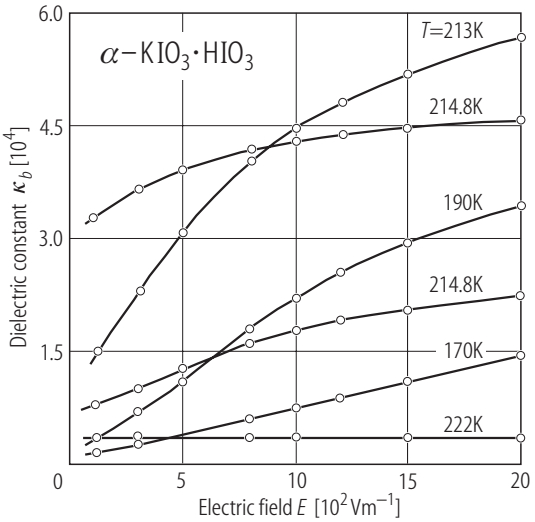

Fig. 32A-3-014. α-$KIO_3 \cdot HIO_3$. κ_b vs. E [91Bai]. Parameter: T. f = 1 kHz. E: intensity of measuring ac electric field. The sequence of the experiment was 222 K → 214.8 K (upper line) → 213 K → 190 K → 170 K → 214.8 K (lower line).

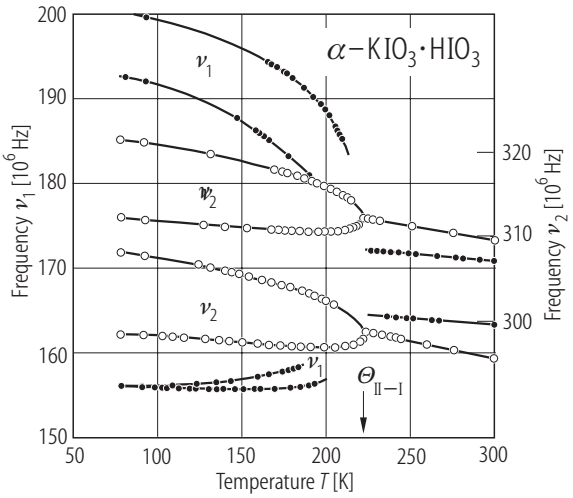

Fig. 32A-3-015. α-$KIO_3 \cdot HIO_3$. ν_1, ν_2 vs. T [78Pet1]. ν_1, ν_2: ^{127}I NQR frequency of (1/2 ↔ 3/2) and (3/2 ↔ 5/2) transition, respectively.

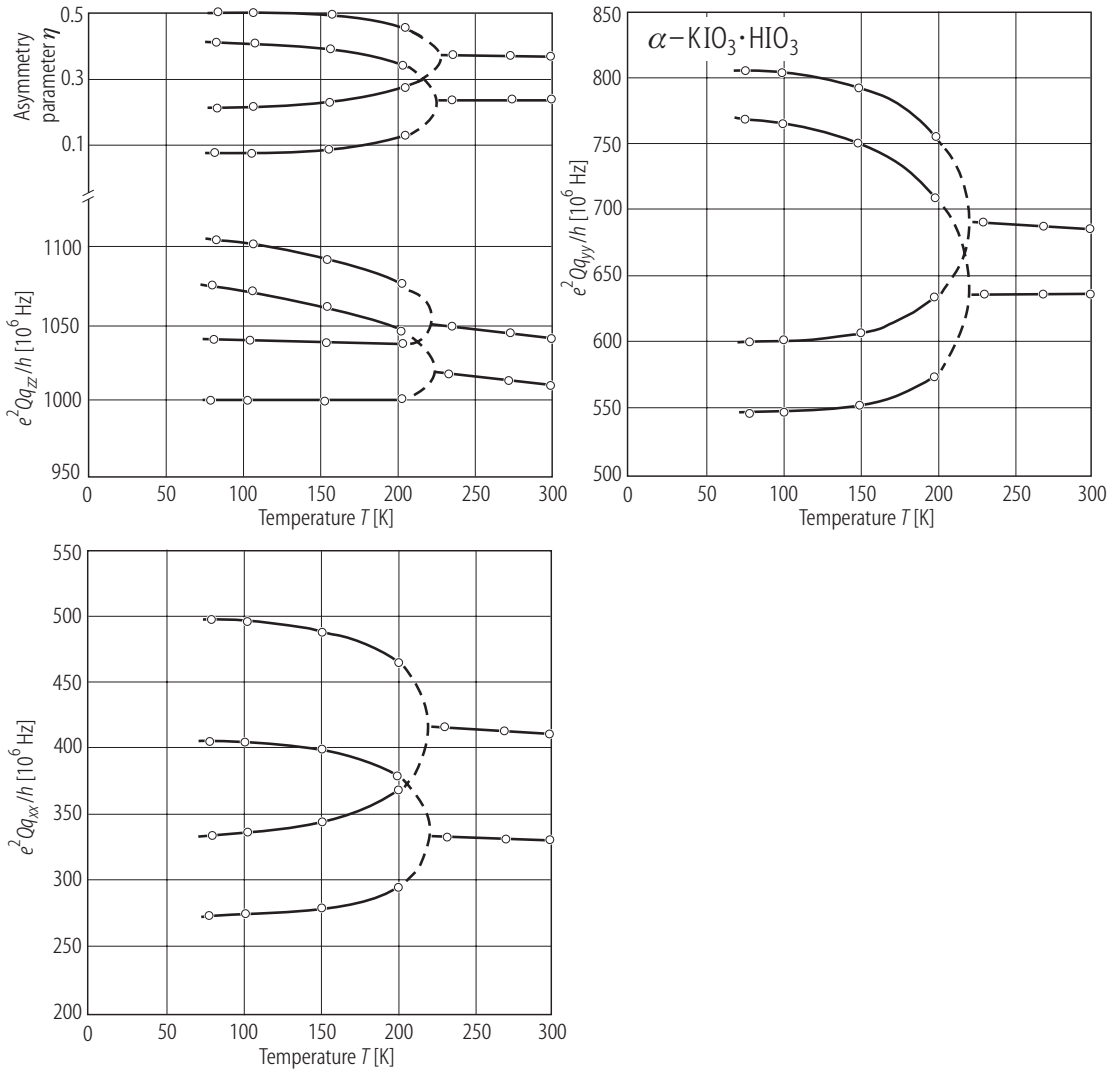

Fig. 32A-3-016. α-KIO_3 · HIO_3. e^2Qq_{zz}/h, e^2Qq_{yy}/h, e^2Qq_{xx}/h and η vs. T [83Pet]. e^2Qq_{zz}/h, e^2Qq_{yy}/h, e^2Qq_{xx}/h: components of nuclear quadrupole coupling tensor of ^{127}I, η: asymmetry parameter.

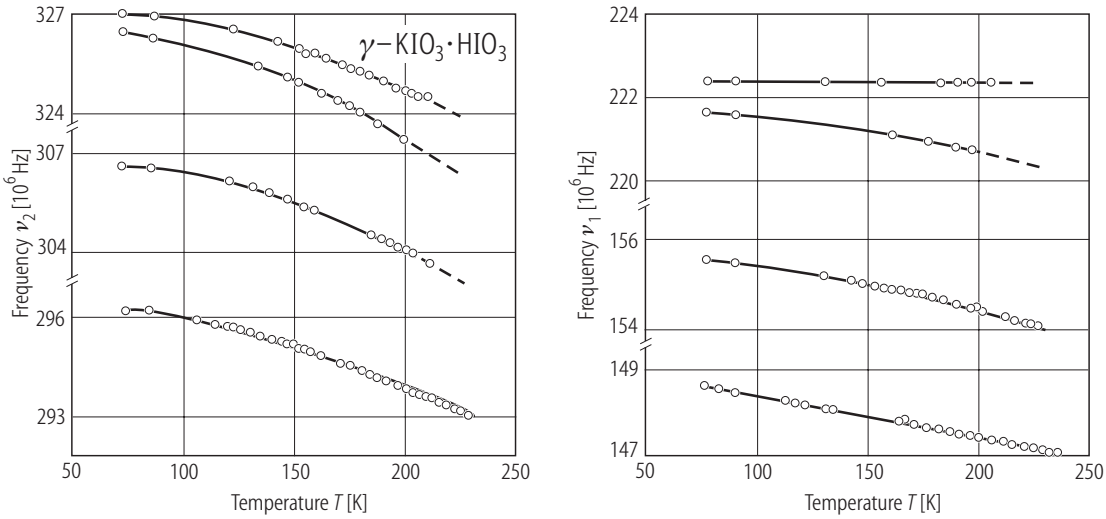

Fig. 32A-3-017. γ-$KIO_3 \cdot HIO_3$. ν_1, ν_2 vs. T [78Pet2]. ν_1, ν_2: ^{127}I NQR frequency of (1/2 ↔ 3/2) and (3/2 ↔ 5/2) transition, respectively.